Signatures of Hyperfine, Spin-Orbit, and Decoherence Effects in a Pauli Spin Blockade

T. Fujita,[1,*] P. Stano,[2,3] G. Allison,[1,2] K. Morimoto,[1] Y. Sato,[1] M. Larsson,[1]
J.-H. Park,[2] A. Ludwig,[4] A. D. Wieck,[4] A. Oiwa,[5] and S. Tarucha[1,2]

[1]*Department of Applied Physics, The University of Tokyo, 7-3-1 Hongo, Bunkyo-ku, Tokyo 113-8656, Japan*
[2]*Center for Emergent Matter Science (CEMS), RIKEN, 2-1 Hirosawa, Wako-shi, Saitama 351-0198, Japan*
[3]*Institute of Physics, Slovak Academy of Sciences, 845 11 Bratislava, Slovakia*
[4]*Lehrstuhl für Angewandte Festkörperphysik, Ruhr-Universität Bochum, Universitätsstraße 150, Gebäude NB, D-44780 Bochum, Germany*
[5]*The Institute of Scientific and Industrial Research, Osaka University, 8-1 Mihogaoka, Ibaraki, Osaka 567-0047, Japan*

(Received 24 February 2016; revised manuscript received 31 August 2016; published 11 November 2016)

We detect in real time interdot tunneling events in a weakly coupled two-electron double quantum dot in GaAs. At finite magnetic fields, we observe two characteristic tunneling times T_d and T_b, belonging to, respectively, a direct and a blocked (spin-flip-assisted) tunneling. The latter corresponds to the lifting of a Pauli spin blockade, and the tunneling times ratio $\eta = T_b/T_d$ characterizes the blockade efficiency. We find pronounced changes in the behavior of η upon increasing the magnetic field, with η increasing, saturating, and increasing again. We explain this behavior as due to the crossover of the dominant blockade-lifting mechanism from the hyperfine to spin-orbit interactions and due to a change in the contribution of the charge decoherence.

DOI: 10.1103/PhysRevLett.117.206802

Electron spins in semiconductor quantum dots are promising resources for quantum information processing [1,2]. Laterally gated dots [3] are especially attractive due to the flexibility and scalability [4] of their design and the possibility to electrically initialize [5], manipulate [6,7], and measure [8,9] the slowly relaxing [10,11] spin states. Pauli spin blockade (PSB) [12] plays a crucial role in electrical manipulations. PSB is established when the conservation of spin blocks a transition from an excited state, where two electrons in two dots have parallel spins, to the ground state, where they form a singlet in one dot. The spin can thus be detected by a local charge sensor as the presence or absence of a charge transition [13–15]. The blockade is lifted by spin flips, limiting the readout fidelities [16,17], as well as manipulations and preparations of quantum states [18,19].

In GaAs quantum dots, there are two important sources of electron spin flips: the spin-orbit coupling and the hyperfine interaction with spins of atomic nuclei. Respectively, they dominate the spin relaxation time T_1 [20,21] and decoherence time T_2 [22–24]. Apart from causing detrimental effects, both of these can be utilized in quantum state manipulation as a means of coupling the electrical control fields to spins [25–28]. It is known that the relative importance of these two effects changes with the magnetic field strength and orientation [19,29,30]. By experimentally resolving the direct and spin-flip-assisted interdot tunneling in real time, here we investigate the limit that these factors impose on the effectiveness of PSB. Upon scanning a large range of a single parameter, the magnetic field, we find a crossover in their dominance. Fully consistent with our theory, these results give guidance on how to increase the PSB effectiveness with importance for spin readout applications. We also note that, different from Refs. [21,31,32], we observe a weakly coupled double dot *at the charge degeneracy point*. This makes the system independent on inelastic transitions whose energy dependence, together with the dynamical nuclear spin polarization, otherwise results in complex behavior due to nonlinearities [33,34].

Our device is a gate-defined lateral double quantum dot (DQD) [Fig. 1(a)] weakly tunnel coupled and isolated from reservoirs, with lead-dot tunneling rates of the order of hertz and the interdot tunneling rate of the order of kilohertz. In this regime, where tunnel coupling energies are much smaller than orbital or charging energies, the two electron configurations span a basis of five states [35,36]: one (02) charge state, the singlet $S(02)$, and four (11) charge states, the two spin-polarized triplets $T_{\pm}(11)$, the unpolarized triplet $T_0(11)$, and the singlet $S(11)$. Here by $(N_L N_R)$ we denote the left and right dot occupancies as N_L and N_R, respectively. Since the exchange energy splitting among the (11) charge

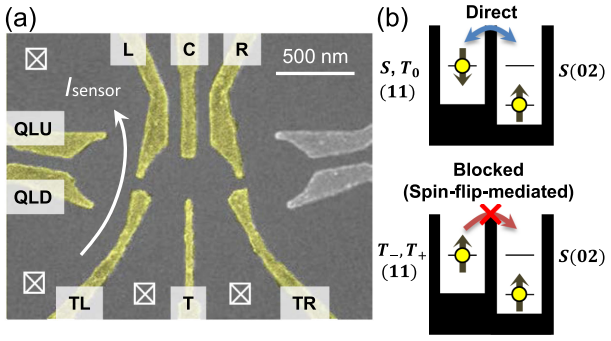

FIG. 1. (a) A scanning electron micrograph of a sample similar to that measured. (b) Schematics of the direct and spin-flip-assisted interdot tunneling.

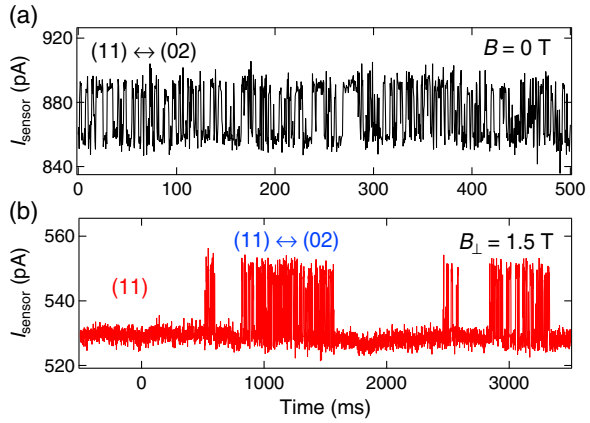

FIG. 2. Typical real time charge sensor signals of a weakly tunnel coupled DQD at the (11)-(02) degeneracy for zero (a) and finite (b) magnetic fields. In (a), the signal shows repeated direct tunneling events, switching the dot between totally mixed spin states in the (11) and the $S(02)$ state. In (b), spin-polarized (11) states are energetically split by a finite field and blocked in the (11) state, having a longer time to tunnel into the $S(02)$ state.

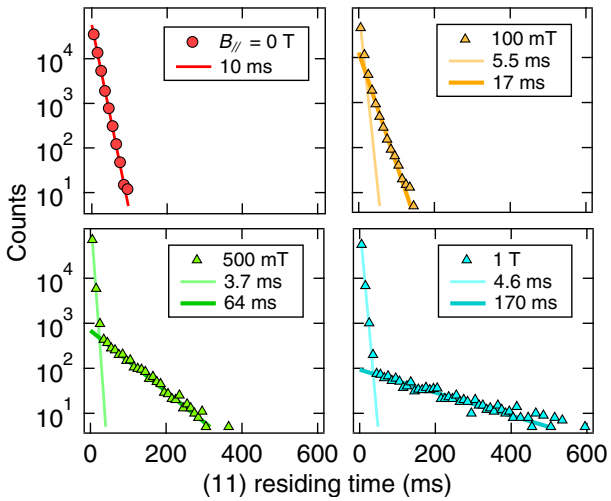

FIG. 3. Example histograms of the (11) charge state residing time for different in-plane magnetic fields. Lines show the fitted linear trend for zero field and at short (T_d) and long (T_b) times for finite fields (see [40] for details of the fitting procedure).

states is negligible, the four (11) states are degenerate and, in general, energetically separated from the $S(02)$ state by the detuning energy Δ. The nearby charge sensor can discriminate different charge states [37]. Using gates L and R, we tune the dot close to the (11)-(02) degeneracy, $\Delta \approx 0$, by balancing the time-averaged occupations of the two charge configurations, and measure the sensor current I_{sensor}. With the interdot tunneling time set above the time resolution of the sensor, we monitor in this way the dot charge configuration in real time.

Figure 2(a) shows a random (thermally excited) switching of charge configurations at zero magnetic field. The histogram of (11) to (02) tunneling times plotted in the upper left panel of Fig. 3 shows that the tunneling is described by a single time constant T, with the probability that no tunneling occurs for time δt being $\exp(-\delta t/T)$. Despite different spin configurations of the (11) states, a single tunneling rate into the (02) singlet is expected due to the hyperfine field of nuclear spins. Indeed, if described as a Zeeman term of a slowly fluctuating classical magnetic field located in the left (right) dot $\mathbf{B}_N^{L(R)}$ [38], these quasistatic random fields, in general, couple all five states. Though the couplings between the (11) and (02) states are negligible, they are appreciable among the (11) states (see below). As a consequence, no matter in which (11) spin state the system starts, within a few nanoseconds it contains the $S(11)$ state with an amplitude of the order of 1 from where it can tunnel to $S(02)$. As a result, within our time resolution, all (11) states tunnel out with the same rate and there is no PSB.

The charge-switching behavior is different at a large enough external magnetic field $\mathbf{B}$; see Fig. 2(b) for $B_\perp = 1.5$ T. In addition to the fast switching as in Fig. 2(a), there are long intervals where the system remains in a (11) state. This is the Pauli spin blockade: Once $B > B_N$, the Zeeman energy offset of the polarized triplets suppresses their hyperfine induced admixture with $S(11)$ and by that their tunneling to $S(02)$. Since $T_0(11)$ still mixes fast with $S(11)$, we expect to see two tunneling times: T_b for spin-flip-assisted tunneling of spin-polarized states and T_d for direct tunneling of spin-unpolarized states. The two processes are sketched on Fig 1(b), and the histograms plotted in Fig. 3 indeed show biexponential distributions for $B_\parallel \geq 100$ mT.

We have investigated this PSB manifestation as a function of the magnetic field strength. In the search for generic features, we measured for various sample cooldowns, which can change the shape of the dot, and for both in-plane and perpendicular magnetic fields, by which we isolate the strong orbital effects of the latter. Because of the influence of the AlGaAs barriers [39], the g factor is small, $|g_\perp| < 0.12$ for an out-of-plane magnetic field, and, as we find from the analysis below, about 5 times smaller for in-plane fields. (These small values make it easier to analyze the behavior of the rates at small Zeeman energies, which are pushed to higher magnetic fields by the small g factors.) Because of variations in the measurement conditions, there is little systematic dependence of the tunneling times taken individually (see Fig. S2 in Ref. [40]). This is mostly due to the exponential sensitivity of the $S(11) - S(02)$ tunneling matrix element τ, which is hard to keep constant during the realignment of the states' energies required in the measurement course. [This is also the reason for an irrelevant overall shift of the sensor current seen comparing Figs. 2(a) and 2(b).] However, in plotting the ratio $\eta = T_b/T_d$ as in Fig. 4, τ drops out and a clear trend emerges.

From zero to moderate external fields, η behaves as expected: Initially equal to one, it offsets once the external field becomes larger than the nuclear field. Here it grows as

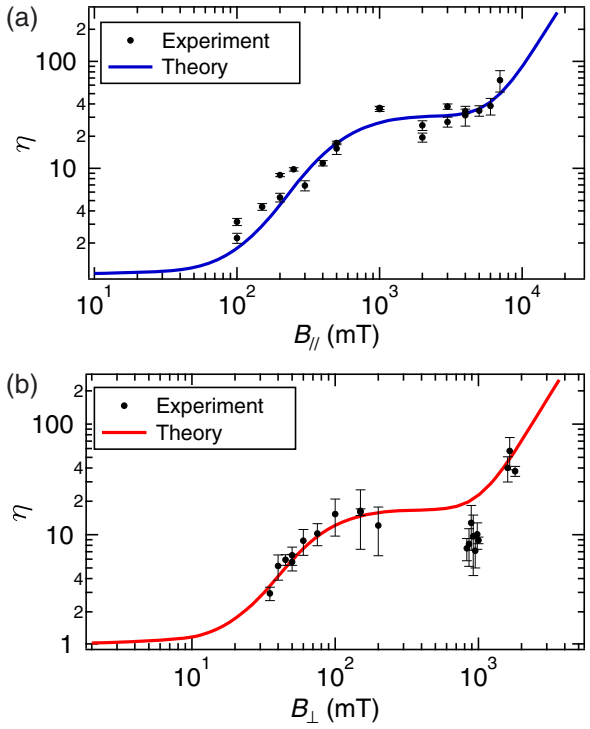

FIG. 4. The ratio of tunneling times η as a function of, respectively, parallel (a) and perpendicular (b) magnetic field. Lines are fits using the model and parameters described in the text. The x axes of the panels are aligned according to the corresponding Zeeman energies.

$\eta \propto (B/B_N)^2$, as is well known [21] and can be understood from a simple perturbation theory (see below). At higher fields, however, we find that the growth stops and η saturates. This is not completely unnatural, as it suggests that the PSB effectiveness is limited by some process, expected to be eventually the case. However, moving to even higher fields, η increases again [63]. This is, however, completely surprising, as it implies that the limitation disappears. It is also at odds with the general behavior of the spin (inelastic) relaxation time T_1 between Zeeman split states, which is known to decrease with the magnetic field (as B^{-5}) as was predicted in theory and confirmed experimentally [10,20].

We now present a theoretical model explaining these observations. At the charge degeneracy point, a regime we explore, the inelastic rates with strong energy dependence, usually due to the phonon density of states, play little role, which is a substantial simplification and difference from some previous experiments. Let us consider several ingredients, namely, the interactions with the external, hyperfine, and spin-orbit fields [64,65]:

$$H = H_0 + H_Z + H_{\rm nuc} + H_{\rm so}. \tag{1}$$

With details in Ref. [40], H_0 describes the double dot and consists of the electron kinetic energy, confinement potential, and Coulomb interaction and defines the Hilbert space as described above, with the (11) states detuned from $S(02)$ by Δ and the two singlets tunnel coupled by $\tau \equiv \langle S(11)|H_0|S(02)\rangle$. The spin-polarized triplets are offset by the Zeeman energy $\pm|g\mu_B B|$, which for our g factors corresponds to 7 μeV for $B_\perp = 1$ T and 1.4 μeV for $B_\parallel = 1$ T. A typical matrix element of $H_{\rm nuc}$ within the (11) subspace is of the order of 0.1 μeV. Finally, assuming $H_{\rm so}$ contains the linear-in-momentum Dresselhaus and Rashba terms, the only nonzero matrix elements are

$$\langle T_\pm(11)|H_{\rm so}|S(11)\rangle = \pm\sqrt{2}g\mu_B B\frac{d}{\lambda_{\rm so}}. \tag{2}$$

Here, $\lambda_{\rm so}$ is an effective spin-orbit length, a combination of the Dresselhaus and Rashba coefficients, and d is half of the interdot distance, which we estimate to be 130 nm from typical values of T_d [40].

The system dynamics is given by the equation for its density matrix ρ:

$$i\hbar\partial_t\rho = [H,\rho] + L[\rho]. \tag{3}$$

The last term is due to charge noise, usually dominated by fluctuating electric fields of phonons, gate potentials, impurities, and the charge sensor current. It leads to a fast decay of charge superpositions, with the decoherence rate Γ, typically several gigahertz [66]. Denoting a (11) state as X, and $S(02)$ as S, the charge decoherence is described by $(L[\rho])_{XS} = -\Gamma\rho_{XS}$, a form independent of the (11) subspace basis. We use this invariance to simplify Eq. (3) by choosing basis states $|X\rangle$ in which H is diagonal within the (11) subspace. Because of the hyperfine and spin-orbit couplings, these eigenstates are, in general, superpositions of all four (11) states. In this basis, the remaining off-diagonal matrix elements are the tunneling terms

$$\tau_{XS} \equiv \langle X|H|S(02)\rangle = \tau\langle X|S(11)\rangle, \tag{4}$$

which are much smaller than the states' energy differences and can be treated perturbatively. In the leading order, the dynamics given by Eq. (3) reduces to transitions between X and S with the rate

$$T_X^{-1} = \frac{2\pi}{\hbar^2}\int d\omega \frac{1}{\pi}\frac{\Gamma}{\Gamma^2 + (\omega-\omega_{XS})^2}H_{XS}^2(\omega). \tag{5}$$

For further convenience, we introduce the spectral density of the transition matrix element

$$H_{XS}^2(\omega) = \frac{1}{2\pi}\int dt\langle X|H(0)|S\rangle\langle S|H(t)|X\rangle\exp(i\omega t). \tag{6}$$

For a time-independent Hamiltonian, which we consider at the moment, $H_{XS}^2(\omega) = |\tau_{XS}|^2\delta(\omega)$. Inserting this into Eq. (5) gives Fermi's golden rule formula with the initial and final state difference $E_X - E_S = \hbar\omega_{XS}$, Lorentzian broadened by the decoherence.

We fit this model to the data in Fig. 4 by averaging the rates given by Eq. (5) over hyperfine fields $\mathbf{B}_N^{L,R}$, assuming the latter having a Gaussian probability distribution with a zero mean value and dispersion B_N^2. The typical hyperfine field

B_N, the charge decoherence rate Γ, and the spin-orbit length λ_{so} are fitting parameters. To take into account the limited accuracy of the detuning and the voltage jitter present in real experiments, we average over $\Delta \in \langle 0, 12\rangle$ μeV, a range corresponding to the electron temperature [67]. However, the influence of Δ on the data fit in Fig. 4 is relatively minor. On the contrary, B_N, Γ, and λ_{so} have a profound influence, and the energy scales connected to these key quantum dot spin qubit parameters can be directly read off from the magnetic field dependence of η, as we now explain.

Let us first assume the detuning is zero, and the hyperfine fields are fixed. We order the four $|X\rangle$ states according to their increasing overlap with $S(11)$. The first state, denoted by label X, represents a typical blocked state, while the last, with label X', a typical unblocked state. Using Eqs. (4)–(6), we get the ratio of tunneling times $X(11) \leftrightarrow S(02)$, $X'(11) \leftrightarrow S(02)$ as

$$\frac{T_X}{T_{X'}} = \frac{\Gamma^2 + \omega_{XS}^2}{\Gamma^2 + \omega_{X'S}^2} \left| \frac{\langle X'|S(11)\rangle}{\langle X|S(11)\rangle} \right|^2. \tag{7}$$

Take first $B = 0$. As already explained, the hyperfine fields fully mix the (11) subspace, so that each eigenstate typically contains the same amount of admixture of $S(11)$. Because in addition the Zeeman energy of hyperfine fields is negligible compared to $\hbar\Gamma$, the ratio in Eq. (7) is 1. Once $B \gg B_N$, the singlet admixture into the Zeeman split triplets is small: $|\langle X|S(11)\rangle|^2 \propto B_N^2/B^2$. The remaining two states, typically equally mixed $S(11)$ and $T_0(11)$, have $|\langle X'|S(11)\rangle|^2 \sim 1/2$. This gives two tunneling times with the ratio proportional to B^2/B_N^2.

The plateau terminating the growth of η at higher fields (around 0.1 T for $B_\perp$) can be understood as the spin-orbit field taking over the hyperfine field in the matrix element in Eq. (4). Indeed, whereas the latter is independent of B, the former grows linearly; see Eq. (2). This equation also gives the spin-orbit length as $\lambda_{so} \sim 2d\sqrt{2\eta}$ with η the ratio on the plateau.

Increasing the magnetic field further (beyond 1 T for $B_\perp$), η starts to grow again in Fig. 4. This can be still reconciled with Eq. (7), as due to the first fraction on its right-hand side. Namely, once the Zeeman energy becomes larger than the decoherence, the spectral overlap of spin-polarized (11) states and $S(02)$ drops compared to spin-unpolarized (11) states. The Zeeman energy where η starts increasing for the second time gives, therefore, the charge decoherence rate $\hbar\Gamma$.

The three energy scales extracted visually as just described from the slope changes of η give the values of parameters B_N, λ_{so}, and Γ within a factor of the order of one. We found that the best way to nail down these factors quantitatively is straightforward numerics. Namely, for given values of hyperfine fields, we diagonalize the 4×4 Hamiltonian in the (11) subspace numerically and calculate the rates according to Eq. (5). We average these over typically 10^6 hyperfine field random configurations. Because we cannot distinguish experimentally all four rates, we define in our numerics the "blocked (direct)" rate as the average of the first (last) two rates ordered by their magnitudes.

In this way, we obtain the solid lines in Fig. 4 using $|g|\mu B_N = 1.7$ μeV, $\Gamma = 7$ GHz, and $\lambda_{so} = 1.1$ μm for the out-of-plane field and $\lambda_{so} = 1.5$ μm for the in-plane field. From the value of B_N, we can infer the number of nuclei within the dot volume [68], $N = [AI(I+1)/g\mu_B B]^2 \approx 1.2 \times 10^5$, using $A = 90$ μeV, and $I = 3/2$. All extracted values are typical for gated dots in GaAs, that is, N [69], the charge decoherence rate [70,71], and spin-orbit lengths [10,72]. We note that the different values of the effective spin-orbit length fitted for in-plane and out-of-plane magnetic fields are consistent with directional anisotropies of λ_{so} [73], observed in dot spectra [19], and spin relaxation [74].

We also considered alternative explanations, examining inelastic (11) to (02) transitions due to a nondipolar electric noise, inelastic (T_1) transitions within the (11) subspace, and lifting the spin blockade by cotunneling. As none of these can be naturally reconciled with the data, we give these details only in Ref. [40].

We conclude by suggesting how to increase the PSB effectiveness. The spin-orbit effects should be minimized, which can be achieved by orienting the magnetic field along certain in-plane directions [75], specified by setting $\lambda_{so}^{-1} = 0$ in Eq. (S23) in Ref. [40]. We predict that the quadratic growth $\eta \sim B^2$ will then extend to much higher fields and increase to B^4 once the Zeeman energy becomes larger than the charge decoherence rate. Finally, these properties are to a large extent independent of the value of the interdot tunneling, an increase of which should therefore boost both direct and blocked rates while preserving their ratio.

Upon completion of this work, we became aware of Ref. [76], where spin-flip-assisted interdot transitions were observed in real time, similar to here. The transition rate ratio saturation, due to the crossover from nuclear to spin-orbit dominance of the tunneling, is confirmed there (at smaller fields due to a larger g factor) with the same interpretation and a similar spin-orbit length, of the order of 1 μm, fitted. Different from our results, Ref. [76] suggests exponential (rather than quadratic) functional dependence of the ratio on the magnetic field below the crossover, does not report on behavior at higher magnetic fields (where we see the second upturn in η), and invokes inelastic spin flips to explain the data.

This work was supported by Grant-in-Aid for Scientific Research S (26220710) and A (25246005), Innovative area (26103004), CREST, JST, ImPACT program, MEXT Project for Developing Innovation Systems and QPEC, The University of Tokyo. T. F. is supported by a JSPS Postdoctoral Fellowship for Research Abroad. P. S. acknowledges the support of APVV-0808-12 (QIMABOS), JSPS KAKENHI Grant No. 16H02204

and 16K05411. A. L. and A. D. W. acknowledge gratefully support of DFG-TRR160 and BMBF-Q.com-H 16KIS0109.

*t.fujita@tudelft.nl

[1] D. Loss and D. P. DiVincenzo, Phys. Rev. A **57**, 120 (1998).
[2] C. Kloeffel and D. Loss, Annu. Rev. Condens. Matter Phys. **4**, 51 (2013).
[3] R. Hanson, L. P. Kouwenhoven, J. R. Petta, S. Tarucha, and L. M. K. Vandersypen, Rev. Mod. Phys. **79**, 1217 (2007).
[4] M. R. Delbecq, T. Nakajima, T. Otsuka, S. Amaha, J. D. Watson, M. J. Manfra, and S. Tarucha, Appl. Phys. Lett. **104**, 183111 (2014).
[5] J. M. Elzerman, R. Hanson, L. H. W. van Beveren, B. Witkamp, L. M. K. Vandersypen, and L. P. Kouwenhoven, Nature (London) **430**, 431 (2004).
[6] M. Pioro-Ladriére, T. Obata, Y. Tokura, Y.-S. Shin, T. Kubo, K. Yoshida, T. Taniyama, and S. Tarucha, Nat. Phys. **4**, 776 (2008).
[7] J. Yoneda, T. Otsuka, T. Nakajima, T. Takakura, T. Obata, M. Pioro-Ladriére, H. Lu, C. J. Palmstr/om, A. C. Gossard, and S. Tarucha, Phys. Rev. Lett. **113**, 267601 (2014).
[8] R. Hanson, L. H. Willems van Beveren, I. T. Vink, J. M. Elzerman, W. J. M. Naber, F. H. L. Koppens, L. P. Kouwenhoven, and L. M. K. Vandersypen, Phys. Rev. Lett. **94**, 196802 (2005).
[9] K. C. Nowack, M. Shafiei, M. Laforest, G. E. D. K. Prawiroatmodjo, L. R. Schreiber, C. Reichl, W. Wegscheider, and L. M. K. Vandersypen, Science **333**, 1269 (2011).
[10] S. Amasha, K. MacLean, I. P. Radu, D. M. Zumbühl, M. A. Kastner, M. P. Hanson, and A. C. Gossard, Phys. Rev. Lett. **100**, 046803 (2008).
[11] H. Bluhm, S. Foletti, I. Neder, M. Rudner, D. Mahalu, V. Umansky, and A. Yacoby, Nat. Phys. **7**, 109 (2011).
[12] K. Ono, D. G. Austing, Y. Tokura, and S. Tarucha, Science **297**, 1313 (2002).
[13] D. J. Reilly, C. M. Marcus, M. P. Hanson, and A. C. Gossard, Appl. Phys. Lett. **91**, 162101 (2007).
[14] M. C. Cassidy, A. S. Dzurak, R. G. Clark, K. D. Petersson, I. Farrer, D. A. Ritchie, and C. G. Smith, Appl. Phys. Lett. **91**, 222104 (2007).
[15] A. Hofmann, V. F. Maisi, C. Gold, T. Krähenmann, C. Rössler, J. Basset, P. Märki, C. Reichl, W. Wegscheider, K. Ensslin, and T. Ihn, following Letter, Phys. Rev. Lett. **117**, 206803 (2016).
[16] C. Barthel, D. J. Reilly, C. M. Marcus, M. P. Hanson, and A. C. Gossard, Phys. Rev. Lett. **103**, 160503 (2009).
[17] C. Barthel, M. Kjaergaard, J. Medford, M. Stopa, C. M. Marcus, M. P. Hanson, and A. C. Gossard, Phys. Rev. B **81**, 161308(R) (2010).
[18] M. D. Shulman, O. E. Dial, S. P. Harvey, H. Bluhm, V. Umansky, and A. Yacoby, Science **336**, 202 (2012).
[19] J. M. Nichol, S. P. Harvey, M. D. Shulman, A. Pal, V. Umansky, E. I. Rashba, B. I. Halperin, and A. Yacoby, Nat. Commun. **6**, 7682 (2015).
[20] A. V. Khaetskii and Y. V. Nazarov, Phys. Rev. B **64**, 125316 (2001).
[21] A. C. Johnson, J. R. Petta, J. M. Taylor, A. Yacoby, M. D. Lukin, C. M. Marcus, M. P. Hanson, and A. C. Gossard, Nature (London) **435**, 925 (2005).
[22] A. V. Khaetskii, D. Loss, and L. Glazman, Phys. Rev. Lett. **88**, 186802 (2002).
[23] J. R. Petta, A. C. Johnson, J. M. Taylor, E. A. Laird, A. Yacoby, M. D. Lukin, C. M. Marcus, M. P. Hanson, and A. C. Gossard, Science **309**, 2180 (2005).
[24] M. R. Delbecq, T. Nakajima, P. Stano, T. Otsuka, S. Amaha, J. Yoneda, K. Takeda, G. Allison, A. Ludwig, A. D. Wieck, and S. Tarucha, Phys. Rev. Lett. **116**, 046802 (2016).
[25] K. C. Nowack, F. H. L. Koppens, Y. V. Nazarov, and L. M. K. Vandersypen, Science **318**, 1430 (2007).
[26] V. Srinivasa, K. C. Nowack, M. Shafiei, L. M. K. Vandersypen, and J. M. Taylor, Phys. Rev. Lett. **110**, 196803 (2013).
[27] S. Foletti, H. Bluhm, D. Mahalu, V. Umansky, and A. Yacoby, Nat. Phys. **5**, 903 (2009).
[28] A. D. Wieck, E. Batke, D. Heitmann, J. P. Kotthaus, and E. Bangert, Phys. Rev. Lett. **53**, 493 (1984).
[29] S. Nadj-Perge, S. M. Frolov, J. W. W. van Tilburg, J. Danon, Y. V. Nazarov, R. Algra, E. P. A. M. Bakkers, and L. P. Kouwenhoven, Phys. Rev. B **81**, 201305 (2010).
[30] M. Raith, P. Stano, F. Baruffa, and J. Fabian, Phys. Rev. Lett. **108**, 246602 (2012).
[31] K. Ono and S. Tarucha, Phys. Rev. Lett. **92**, 256803 (2004).
[32] F. H. L. Koppens, J. A. Folk, J. M. Elzerman, R. Hanson, L. H. W. van Beveren, I. T. Vink, H. P. Tranitz, W. Wegscheider, L. P. Kouwenhoven, and L. M. K. Vandersypen, Science **309**, 1346 (2005).
[33] M. S. Rudner, F. H. L. Koppens, J. A. Folk, L. M. K. Vandersypen, and L. S. Levitov, Phys. Rev. B **84**, 075339 (2011).
[34] S. Sharmin, K. Muraki, and T. Fujisawa, Phys. Rev. B **89**, 115315 (2014).
[35] W. A. Coish and D. Loss, Phys. Rev. B **72**, 125337 (2005).
[36] D. Stepanenko, M. Rudner, B. I. Halperin, and D. Loss, Phys. Rev. B **85**, 075416 (2012).
[37] T. Fujita, H. Kiyama, K. Morimoto, S. Teraoka, G. Allison, A. Ludwig, A. D. Wieck, A. Oiwa, and S. Tarucha, Phys. Rev. Lett. **110**, 266803 (2013).
[38] I. Neder, M. S. Rudner, H. Bluhm, S. Foletti, B. I. Halperin, and A. Yacoby, Phys. Rev. B **84**, 035441 (2011).
[39] G. Allison, T. Fujita, K. Morimoto, S. Teraoka, M. Larsson, H. Kiyama, A. Oiwa, S. Haffouz, D. G. Austing, A. Ludwig, A. D. Wieck, and S. Tarucha, Phys. Rev. B **90**, 235310 (2014).
[40] See Supplemental Material at http://link.aps.org/supplemental/10.1103/PhysRevLett.117.206802 for the details on device structure, data analyses, and theoretical calculations, which includes Refs. [40–61].
[41] P. L. Jeune, D. Robart, X. Marie, T. Amand, M. Brousseau, J. Barrau, V. Kalevich, and D. Rodichev, Semicond. Sci. Technol. **12**, 380 (1997).
[42] S. Amasha, K. MacLean, I. P. Radu, D. Zumbühl, M. Kastner, M. Hanson, and A. Gossard, Phys. Rev. Lett. **100**, 046803 (2008).
[43] P. Stano and J. Fabian, Phys. Rev. B **74**, 045320 (2006).

[44] A. C. Johnson, J. R. Petta, C. M. Marcus, M. P. Hanson, and A. C. Gossard, Phys. Rev. B **72**, 165308 (2005).
[45] T. Fujita, H. Kiyama, K. Morimoto, S. Teraoka, G. Allison, A. Ludwig, A. D. Wieck, A. Oiwa, and S. Tarucha, Phys. Rev. Lett. **110**, 266803 (2013).
[46] K. Morimoto, T. Fujita, G. Allison, S. Teraoka, M. Larsson, H. Kiyama, S. Haffouz, D. G. Austing, A. Ludwig, A. D. Wieck, A. Oiwa, and S. Tarucha, Phys. Rev. B **90**, 085306 (2014).
[47] I. L. Aleiner and V. I. Fal'ko, Phys. Rev. Lett. **87**, 256801 (2001).
[48] E. I. Rashba, Phys. Rev. B **68**, 241315 (2003).
[49] F. Baruffa, P. Stano, and J. Fabian, Phys. Rev. Lett. **104**, 126401 (2010).
[50] F. Baruffa, P. Stano, and J. Fabian, Phys. Rev. B **82**, 045311 (2010).
[51] P. Stano, J. Fabian, and Ph. Jacquod, Phys. Rev. B **85**, 241301(R) (2012).
[52] P. L. Jeune, D. Robart, X. Marie, T. Amand, M. Brousseau, J. Barrau, V. Kalevich, and D. Rodichev, Semicond. Sci. Technol. **12**, 380 (1997).
[53] S. Amasha, K. MacLean, I. P. Radu, D. Zumbühl, M. Kastner, M. Hanson, and A. Gossard, Phys. Rev. Lett. **100**, 046803 (2008).
[54] P. Stano and J. Fabian, Phys. Rev. B **74**, 045320 (2006).
[55] A. C. Johnson, J. R. Petta, C. M. Marcus, M. P. Hanson, and A. C. Gossard, Phys. Rev. B **72**, 165308 (2005).
[56] T. Fujita, H. Kiyama, K. Morimoto, S. Teraoka, G. Allison, A. Ludwig, A. D. Wieck, A. Oiwa, and S. Tarucha, Phys. Rev. Lett. **110**, 266803 (2013).
[57] K. Morimoto, T. Fujita, G. Allison, S. Teraoka, M. Larsson, H. Kiyama, S. Haffouz, D. G. Austing, A. Ludwig, A. D. Wieck, A. Oiwa, and S. Tarucha, Phys. Rev. B **90**, 085306 (2014).
[58] I. L. Aleiner and V. I. Fal'ko, Phys. Rev. Lett. **87**, 256801 (2001).
[59] E. I. Rashba, Phys. Rev. B **68**, 241315 (2003).
[60] F. Baruffa, P. Stano, and J. Fabian, Phys. Rev. Lett. **104**, 126401 (2010).
[61] F. Baruffa, P. Stano, and J. Fabian, Phys. Rev. B **82**, 045311 (2010).
[62] P. Stano, J. Fabian, and Ph. Jacquod, Phys. Rev. B **85**, 241301(R) (2012).
[63] We can reach the last upturn in the trend unequivocally only for out-of-plane fields, where the g factor, and the corresponding Zeeman energy, is 5 times larger than for the in-plane field, even though we are limited to below $B_\perp < 1.5$ T by strong orbital effects.
[64] O. N. Jouravlev and Y. V. Nazarov, Phys. Rev. Lett. **96**, 176804 (2006).
[65] J. Danon and Y. V. Nazarov, Phys. Rev. B **80**, 041301(R) (2009).
[66] K. D. Petersson, J. R. Petta, H. Lu, and A. C. Gossard, Phys. Rev. Lett. **105**, 246804 (2010).
[67] Our resolution is limited due to the finite electron temperature (100 mK), gate potential resolution (1 μeV), and device stability. A small offset $\Delta = k_B T \ln 4$ is expected because of the fourfold difference in the spin degeneracy of the (11) and (20) charge states.
[68] I. A. Merkulov, A. L. Efros, and M. Rosen, Phys. Rev. B **65**, 205309 (2002).
[69] J. M. Taylor, J. R. Petta, A. C. Johnson, A. Yacoby, C. M. Marcus, and M. D. Lukin, Phys. Rev. B **76**, 035315 (2007).
[70] T. Hayashi, T. Fujisawa, H. D. Cheong, Y. H. Jeong, and Y. Hirayama, Phys. Rev. Lett. **91**, 226804 (2003).
[71] J. R. Petta, A. C. Johnson, C. M. Marcus, M. P. Hanson, and A. C. Gossard, Phys. Rev. Lett. **93**, 186802 (2004).
[72] D. M. Zumbühl, J. B. Miller, C. M. Marcus, K. Campman, and A. C. Gossard, Phys. Rev. Lett. **89**, 276803 (2002).
[73] P. Stano and J. Fabian, Phys. Rev. Lett. **96**, 186602 (2006).
[74] P. Scarlino, E. Kawakami, P. Stano, M. Shafiei, C. Reichl, W. Wegscheider, and L. M. K. Vandersypen, Phys. Rev. Lett. **113**, 256802 (2014).
[75] O. Malkoc, P. Stano, and D. Loss, Phys. Rev. B **93**, 235413 (2016).
[76] V. F. Maisi, A. Hofmann, M. Röösli, J. Basset, C. Reichl, W. Wegscheider, T. Ihn, and K. Ensslin, Phys. Rev. Lett. **116**, 136803 (2016).